Regional Studies in Marine Science 39 (2020) 101467

Contents lists available at ScienceDirect

Regional Studies in Marine Science

journal homepage: www.elsevier.com/locate/rsma

Salt wedge intrusion modeling along the lower reaches of a Mediterranean river

Konstantinos Zachopoulos, Nikolaos Kokkos, Georgios Sylaios *

Laboratory of Ecological Engineering and Technology, Department of Environmental Engineering, Democritus University of Thrace, Vas. Sofias 12, 67100 Xanthi, Greece

ARTICLE INFO

Article history:
Received 25 November 2019
Received in revised form 22 August 2020
Accepted 12 September 2020
Available online 15 September 2020

Keywords:
Strymon River
ELCOM model
Two-layer flow
Arrested salt wedge
Saline water intrusion

ABSTRACT

A three-dimensional numerical model was used to simulate the dynamics of a salt-wedge intruding along the lower Strymon River mouth (northern Greece). The area is microtidal and under the summer increased freshwater demand for irrigation, Strymon outflux at the mouth reduces to near zero. Forcing at boundaries was provided a) from the e-HYPE hydrological model, at the upstream river boundary; b) from the TPXO tidal model, imposed at the open sea boundary, c) from CMEMS for water temperature and salinity open sea profiles, and d) from NOAA-GDAS for meteorological forcing. The model was calibrated with field measurements during summer 2003 and produced fairly reliable results of salt wedge intrusion during summer 2004. The coefficient of determination for salinity reached 0.95; higher correlation was exhibited at the river upstream. Model results underestimated slightly the velocity and salinity along-channel observations. Salt wedge enters the lower river channel in late May 2004, under limited river discharge (< 10 m^3/s) and intrudes up to 4.6 km upstream. The wedge length is controlled by the low river flow, the microtidal domain and complex bottom topography. Logarithmic and power law expressions were derived relating saline water intrusion length (L_{30}) and Strymon River discharge from validated model results. Retention time (RT) calculated based on model outputs varies in Strymon salt wedge between 10 and 20 days. Future work includes the operationalization of Strymon salt wedge model to produce reliable salinity and velocity forecasts along the lower channel.

1. Introduction

River mouths are "traditionally the terminal parts of a river and the regions where lighter river water meets denser sea water and intense mixing occurs" (Pritchard, 1967). Mixing, circulation and maintenance of vertical stratification between fresh and salt water along the lower river channel is governed mainly by river outflows as well as, forces induced by the action of tides, waves and wind (Monbet, 1992; Sierra et al., 2002; Hume et al., 2007). In the micro-tidal Mediterranean environment, the low river discharge (during dry months), the lack of strong tidal currents and the absence of tide-induced turbulence induces limited vertical mixing at the fresh-to-salt water interface (Geyer and Ralston, 2011). Under such conditions, at the lower reaches of river channels with riverbeds below mean sea level, a bidirectional, two-layer flow system is established, characterized by an upper layer of thinner river water flowing downstream towards the river mouth over a lower layer of heavier saltwater advancing upstream (Fischer et al., 1979; Ibañez et al., 1997; Valle-Levinson, 2010). Geyer and MacCready (2014) expanded the traditional Hansen and Rattray Jr (1966) classification scheme by mapping such flows according to the ratio between the freshwater inflow and tidal dynamics, thus differentiating between permanent and time-dependent salt wedges, expressed at spring–neap timescales. In this classification scheme, Strymon River exhibits similar characteristics to Ebro River, in which the salt wedge is formed due to the weak freshwater forcing. Indeed, in Strymon, such regime remains established from early spring to late summer, when low buoyancy inflows prevail; being washed away during the winter higher river flows (Haralambidou et al., 2010). The dominant pattern is a sharp density interface, governed by the sharp halocline, configuring the salt wedge. Its mean position is determined by the balance between the baroclinic pressure gradient due to longitudinal density difference and the opposing river streamflow (Sargent and Jirka, 1987). Under steadily limited river discharge conditions, an "arrested salt wedge" arises, characterized by an active upper fresh water layer and a stagnant lower layer with higher salinity (Chanson, 2004). A number of Mediterranean rivers meet the appropriate conditions for salt wedge formation and upstream intrusion, like the Ebro River in Spain (Ibañez et al., 1997; Sierra et al., 2004), the Rhone river in France (Ibañez et al., 1997), the Neretva (Ljubenkov and Vranješ, 2012), the Jadro (Ljubenkov, 2015) and the Rječina rivers in Croatia (Krvavica et al., 2017b), and the rivers Louros (Scoullos and

* Corresponding author.
E-mail address: gsylaios@env.duth.gr (G. Sylaios).

https://doi.org/10.1016/j.rsma.2020.101467

Table 1
Characteristics of river mouths experiencing a salt wedge.

River	Country	River length (km)	Mean annual river flow (m^3/s)	Intrusion length (km)	Tidal range	Reference
Ebro	Spain	920	<320	>30	Microtidal	Ibañez et al. (1997); Sierra et al. (2004)
Rhone	France	816	~1700	>30	Microtidal	Ibañez et al. (1997)
Neretva	Croatia	225	355	~25	Microtidal	Ljubenkov and Vranješ (2012)
Jadro	Croatia	4.5	7.9	0.91	Microtidal	Ljubenkov (2015)
Rječina	Croatia	18	~10	<0.8	Microtidal	Krvavica et al. (2017b,a)
Louros	Greece	80	~20	n.a	Microtidal	Scoullos and Oldfield (1986)
Acheloos	Greece	220	~140	~3	Microtidal	Dassenakis et al. (1997)
Strymon	**Greece**	**392**	**~59.5**	**~5**	**Microtidal**	Haralambidou et al. (2010)
Mississippi	U.S.A.	3730	~16700	190	Microtidal	McAnally and Pritchard (1997)
Hillsborough	U.S.A.	97	n.a	~12	Mesotidal	Chen et al. (2000)
Douro	Portugal	897	~420	~6	Mesotidal	Vieira and Bordalo (2000)
Yura	Japan	146	~50	~15	Microtidal	Kasai et al. (2010)
Fraser	Canada	3000	120	>20	Mesotidal	MacCready and Geyer (2001)
Merrimack	USA	220	220	>6	Mesotidal	Ralston et al. (2010)

Oldfield, 1986), Acheloos (Dassenakis et al., 1997) and Strymon in Greece (Parissis et al., 2001; Haralambidou et al., 2005, 2010). Salt wedge intrusion also occurs in other rivers outside the Mediterranean basin, with limited to higher effect of tidal action such as the Yura River in Japan (Kasai et al., 2010), the Fraser River in west coast of British Columbia in Canada (MacCready and Geyer, 2001), the Douro River in Portugal (Vieira and Bordalo, 2000). In the U.S.A., the Merrimack river in north east coast of Massachusetts (Ralston et al., 2010), the Hillsborough River (Chen et al., 2000) and the Mississippi River, where the maximum length of the salt wedge was reported, reaching as far as 190 km (McAnally and Pritchard, 1997) (Table 1).

In the Mediterranean arid-in-climate micro-tidal environment, freshwater flow regulation from river damming, river water abstraction and the overall water resources mismanagement and over-use by farmers leads to the summer decline in runoff favoring salt wedge intrusion. As the wedge interacts with bottom topography, downstream river dredging and sand/silt removal and other hydraulic modifications affect salt water intrusion characteristics and the salt wedge shape upstream the river channel (Graas and Savenije, 2008). The salt wedge formation along the lower river mouth triggers a series of adverse environmental effects. The saline wedge intrudes not only longitudinally along the river mouth, but also laterally, salinizing coastal groundwater and degrading nearby aquifers (Barlow, 2003). The long-term isolation of the lower saline layer prohibits the vertical transfer of dissolved oxygen to the bottom stagnant layer (Watanabe et al., 2014). Such event gradually leads to bottom anoxia, deteriorating river water quality (D'Adamo and Lukatelich, 1985). Decline in benthic dissolved oxygen level could be associated with changes in sediment redox and the consequent release of nutrients and trace metals (McAuliffe et al., 1993). Additionally, during tidal floods the enhanced bottom velocities of the salt wedge induce local resuspension and suspended matter flocculation, favoring the occurrence of a turbidity maximum at the tip of the wedge (Sierra et al., 2002; Haralambidou et al., 2010). Sudden salt water intrusions, anoxic events and the presence of turbidity maximum at river bottom affect the abundance and distribution of benthic flora and fauna organisms along the river mouth (Sylaios et al., 2006).

Several approaches have been applied to simulate the behavior and the dynamics of salt wedge in Mediterranean region; regression methods, empirical expressions, physical models, 1D, 2D and more rare 3D numerical models (Ibañez et al., 1997; Haralambidou et al., 2010; Ljubenkov and Vranješ, 2012; Ljubenkov, 2015; Krvavica et al., 2017a). Focusing on the Greek region, very limited publications exist on the hydrodynamic modeling of salt wedge propagation along Greek river mouths under limited discharge conditions. The present research aims to simulate the behavior and dynamics of the Strymon River salt wedge, developing under low river flow conditions, using a three-dimensional hydrodynamic model, calibrated and validated by field measurements. This research could consist a valuable tool in the hands of local authorities in order to handle the salt water intrusion, reducing the environmental and economic impacts on agriculture when considering the effects of climate change. Understanding the processes controlling the formation and intrusion of this seasonally well stratified salt wedge could lead to the better management of upstream water resources. At a further step the model could become operational serving as a tool for the day-to-day salt wedge forecast. The main novelty of this study lies in the use of freely-available hydrologic and hydrodynamic data extracted from existing reliable databases (like e-HYPE, CMEMS, TPXO, and NCEP-GDAS), imposed as boundary conditions at the open boundaries of Strymon River lower channel. This tool could be easily replicable to other estuary environments, with only limitation the accurate bathymetric mapping.

2. Materials and methods

2.1. Study area description

Strymon is a transboundary river sharing its water between North Macedonia, Bulgaria and Greece. It is 392 km long, draining a catchment of 17,330 km^2. The river enters Greece through the Serres plain, and then follows a course of 118 km and eventually outflows into the Strymonikos Gulf, in the Northern Aegean Sea (Fig. 1). The main controller of river discharge is the man-made biotope of Kerkini Lake located 77 km upstream of Strymon River mouth. Kerkini is a man-controlled reservoir storing the river water for irrigation. Strymon has an annually-mean discharge of 59.5 m^3/s; however, during the period of increased irrigation demand (May to September) the lowland river flows almost zeros (Sylaios et al., 2006). Recent findings illustrate that in the latest decades the total freshwater input to the Strymonikos Gulf decreased by about 30% due to the extended use of river water for irrigation and the lower precipitation (Sylaios et al., 2006).

Such changes in the hydrologic regime of the river have led to remarkable changes in the coastal circulation and renewal of Strymonikos Gulf while favoring the occurrence of a salt-wedge intruding upstream the lower river channel (Haralambidou et al., 2005, 2010). Sea water intrudes easily into the river, since the riverbed lies below the sea surface, for a distance up to approximately 9 km upstream from the river mouth (Haralambidou et al., 2003). The present study focuses on the lower river system, characterized as micro-tidal, with tidal amplitudes ranging from 0.30 m in spring tide to 0.14 m in neaps. Mean water depth is approximately 3.5 m, varying between 1.5 and 5 m, and the mean width of the river channel is about 64 m, varying from 40 to 90 m along the channel.

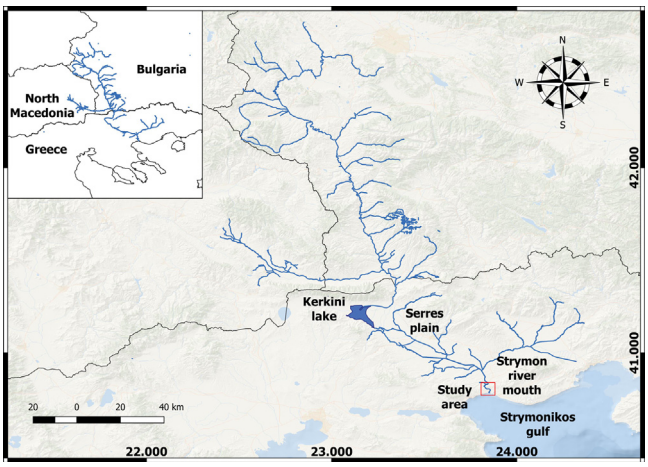

Fig. 1. The hydrographic network of the transboundary Strymon River and the study area (in red square) of Strymon River mouth.

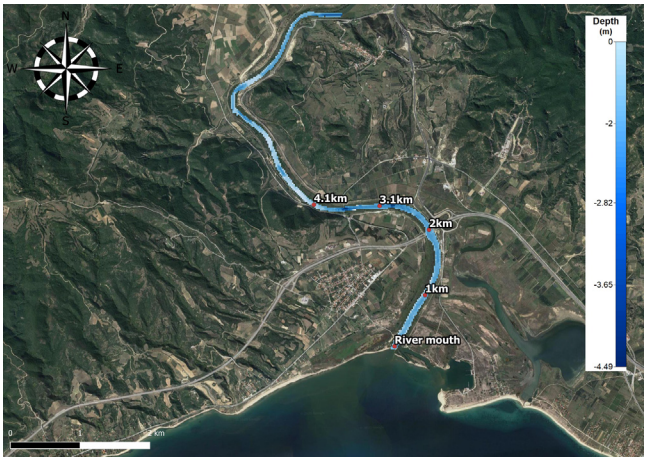

Fig. 2. Strymon River lower channel bathymetry and points of in-situ data collection for model calibration and validation.

2.2. Bathymetry and lower river channel discretization

In-situ river depth measurements were carried out during a hydrographic survey along the Strymon River mouth in 2003 and 2004 summer periods (Haralambidou et al., 2010). Measured depth values were imported into a Geographic Information System (Quantum GIS) and nearest neighbor interpolation was applied leading to the extraction of bathymetry along the lower river channel (Fig. 2).

The computational grid was created using the Vertical Mapper GIS toolkit, capable to produce grid files or continuous information surfaces interpolating data points and calculating the values of grid cells between known points. The horizontal computational domain of the applied three-dimensional model comprised of a discretized rectangular grid of 254 × 149 horizontal cells with a resolution of 20 m × 20 m (Fig. 3a). Such configuration allowed the accurate representation of estuarine complex bathymetry and topography and the reproduction of the physical interchange characteristics of the river. For the vertical discretization, a grid of 55 layers was created, covering the whole water column with a thickness of 0.10 m each, aiming to resolve the sharp halocline interface of the wedge (Fig. 3b). This detailed grid was more appropriate to describe in higher accuracy the geometric characteristics of the salt wedge interface and perform direct correlations between model results and in-situ measurements, aiding model calibration and validation. The total computational domain consisted in total of 2,081,530 computational cells. The vertical grid is flexible at sea surface to accommodate the sea level changes due to tidal oscillations. The river mouth is defined as the lower open boundary, where the open sea data of CMEMS cell were spatially and temporarily interpolated and used as boundary conditions.

2.3. Description of the hydrodynamic numerical model

The Estuary Lake and Coastal Ocean Model (ELCOM) is the three-dimensional hydrodynamic model applied for the simulation of Strymon River salt wedge intrusion (Hodges, 2000; Hodges and Dallimore, 2006). The model has been developed by the Center for Water Research of the University of Western Australia. The model solves the time-varying Navier–Stokes equations, using Reynolds averages, as well as the transmission and diffusion equations using the Boussinesq approach, while eliminating the non-hydrostatic pressure conditions. The most interesting characteristic of ELCOM model is the use of a mixed-layer model, rather than an eddy-diffusivity model, to quantify vertical mixing. This mixed-layer model is more appropriate in highly-stratified flows, as the salt wedges. The mixing process is modeled on a layer-by-layer basis, by comparing the available mixing energy from convective overturns, shear production, wind stirring, and stored mixing energy to the potential energy increase required to mix a grid cell up into the mixed layer above itself (Hodges, 2000; Hodges and Dallimore, 2006). ELCOM numerical approach applies a semi-interlace finite volume scheme on an Arakawa C grid, implementing the TRIM solution (Casulli and Cheng, 1992), with modifications for scalar conservation, numerical diffusion and implementation of a mixed-layer turbulence closure. Convective terms are calculated using a third order Euler–Lagrange scheme, while the ULTIMATE-QUICKEST scheme is introduced for the advection of scalars (Hodges and Dallimore, 2006).

The model reproduces adequately the dynamics of stratified water bodies under external environmental forcing, such as tide, winds, surface heat fluxes and river inflows (Hodges and Dallimore, 2006). Robson and Hamilton (2004) used the ELCOM model to simulate the salt wedge dynamics of Swan River; Ranmadugala (2004) modeled the wedge in Kelani River and Marti and Imberger (2015) in the Swan-Caning Estuary. Therefore, this model seems appropriate for the successful modeling of salt wedge propagation along the Strymon River mouth.

2.4. Initial and boundary conditions

The 3D numerical model of the Strymon River mouth was executed with a time-step of 20 s to simulate in hindcast mode the hydrodynamics of two-years with intense field data (years 2003 and 2004). A “cold start” was initially imposed, with river salinity along the channel arbitrarily set to 0.1 psu and initial freshwater temperature to 15.3 °C. These conditions imply the presence of freshwater throughout the river channel, conditions representing early spring months (March–April) when the wedge is absent. After a warm up period of 2 years, adequate to establish the initial flow and salinity fields, the model was initiated.

Haralambidou et al. (2010) performed 11 sampling surveys and collected vertical profiles of hydrographic (temperature, salinity, and velocity) and water quality data (nutrients concentration, dissolved oxygen content, turbidity and pH) during the summer period of years 2003 and 2004, along the Strymon river lower channel, up to 6.1 km upstream. Each survey involved three to four successive up-estuary transects along the channel’s centerline, collecting data with 500 m horizontal spacing and ranging vertical increments from 0.1 to 0.25 m.

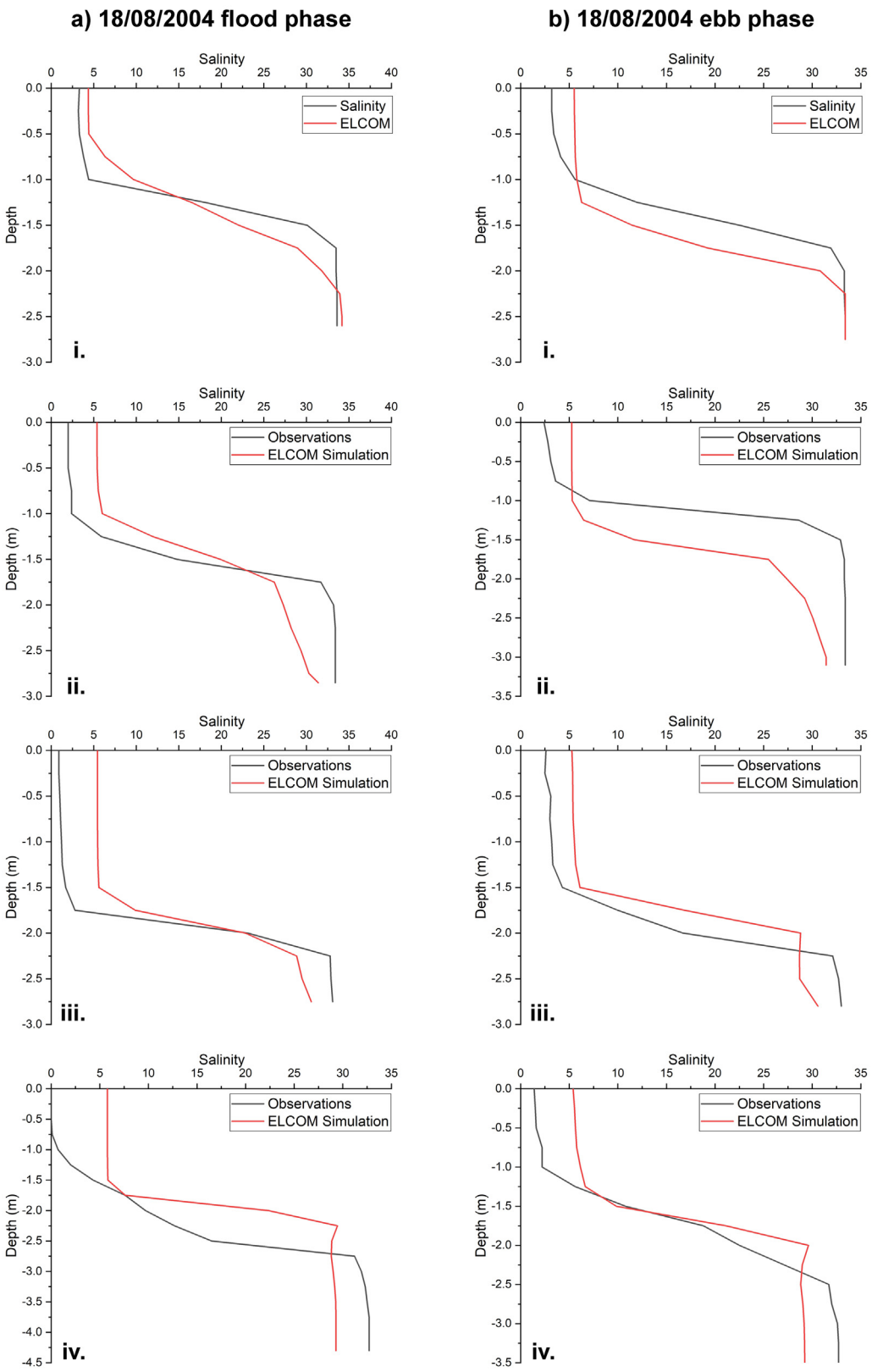

Fig. 3. Salinity profiles from ELCOM simulation (red lines) and field observations (black lines) during (a) the flood phase and (b) the ebb phase on August 18, 2004, at four stations along the Strymon River: (i) at the sea boundary, (ii) 1 km, (iii) 2 km, and (iv) 3.1 km upstream of Strymon River mouth. (For interpretation of the references to colour in this figure legend, the reader is referred to the web version of this article.)

In-situ data from year 2003 were used for model calibration, while data from year 2004 for model validation. Daily mean river discharge data were retrieved from the e-HYPE numerical model database (Lindström et al., 2010; Donnelly et al., 2016) and were imposed at the upstream river flow boundary. These data appear in agreement with the sparse river flow data of Haralambidou

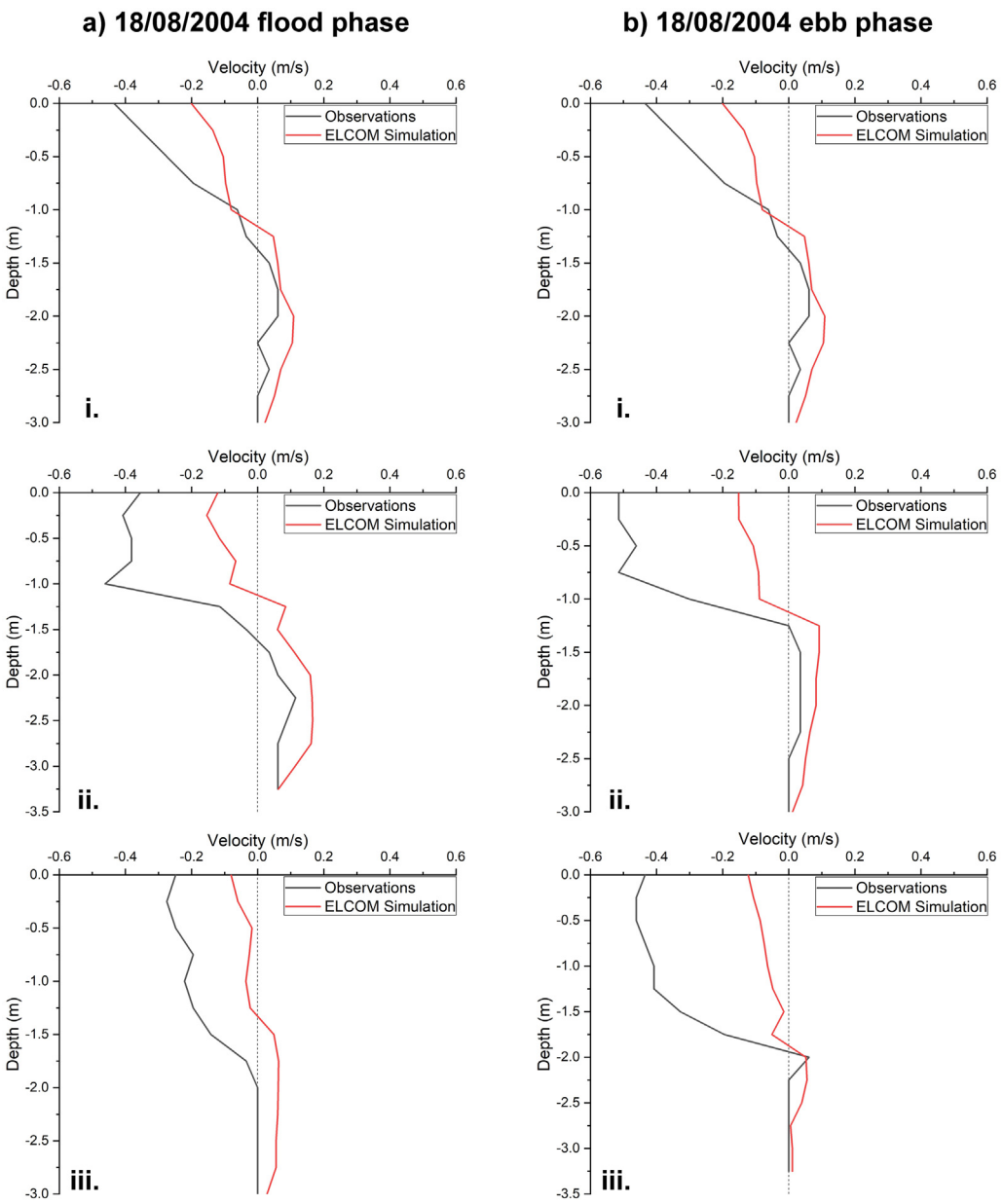

Fig. 4. Velocity profiles from ELCOM simulation (red lines) and field observations (black lines) during (a) the flood phase and (b) the ebb phase on August 18, 2004, at three stations along the Strymon River: (i) at the sea boundary, (ii) 1 km, and (iii) 3.1 km upstream of Strymon River mouth. Negative velocity values indicate water flowing seawards while positive represent an upstream flow. (For interpretation of the references to colour in this figure legend, the reader is referred to the web version of this article.)

et al. (2010) study ($R^2 = 0.76$). Moreover, temperature and salinity in-situ data of the sampling point 6.1 km upstream the river mouth were linearly interpolated to fit the vertical grid ($\Delta z = 0.1$ m) of the model and used as boundary conditions in the upper open boundary. Tidal data from TPXO model (http://volkov.oce.orst.edu/tides/global.html) and temperature and salinity profiles from the Copernicus Marine Environmental Service (CMEMS, http://marine.copernicus.eu/) were imposed at the open oceanic boundary of the river mouth. Meteorological data (wind speed and direction) were derived from the NOAA Global Data Assimilation System (GDAS, https://www.ncdc.noaa.gov/data-access/model-data/model-datasets/global-data-assimilation-system-gdas) database and were imposed over the sea surface of the channel.

Table 2
Dates and observation points used for the ELCOM model validation.

Dates	Observation points
16 Jul 2004	a, b, c, d
25 Jul 2004	a, b, c, d, e
31 Jul 2004	a, b, c, d, e
18 Aug 2004	a, b, c, d
28 Aug 2004	a, b, c

a) near river mouth, b) 1 km upstream, c) 2 km upstream, d) 3.1 km upstream and e) 4.1 km upstream.

2.5. Model calibration and validation procedure and criteria

Model calibration involved the fine-tuning of the drag bottom coefficient (C_D) and the horizontal eddy diffusivity coefficient (N_h) in 2003. More precisely, using the "trial and error" approach at

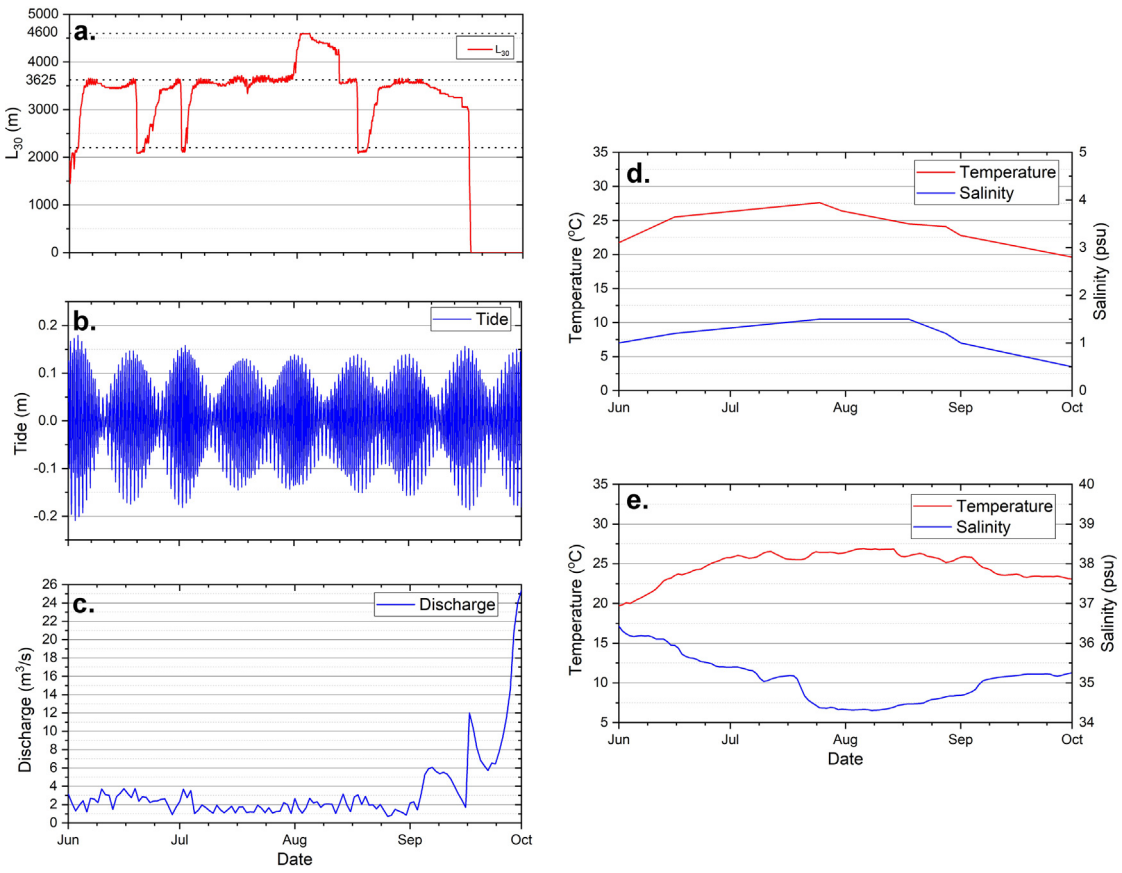

Fig. 5. Variability of (a) the salt wedge length (L_{30}), in relation to (b) the tidal range (in m) at the open boundary, (c) the Strymon River discharge (in m^3/s) at the upstream boundary, (d) the temperature and salinity change at the upstream, and (e) at the open ocean boundaries.

five points along the river channel, the model salinity vertical profile results were related to the respective field measurements for summer 2003 (Haralambidou et al., 2010) (Fig. 2 and Table 2). The best fitted value for the horizontal eddy diffusivity coefficient was $N_h = 0.6$ m^2/s, for the drag bottom coefficient was $C_D = 0.002$.

To assess the validity of model results with in-situ data during model calibration and validation, a set of criteria was established and imposed on the modeled and observed salinity profile data:

(a) The slope (γ), produced by the linear regression on the scatter plot between measured and simulated values. The form of that line is:

$$o_i = \gamma \cdot m_i \quad (1)$$

where $\boldsymbol{m_i}$ and $\boldsymbol{o_i}$ are the modeled and the observed values, respectively.

(b) The coefficient of determination (r^2), assessing the interpretive power of the linear model, expressed as:

$$r^2 = \left(\frac{\sum_{i=1}^{n} (o_i - \overline{o}_i)(m_i - \overline{m}_i)}{\sqrt{\sum_{i=1}^{n} (o_i - \overline{o}_i)^2 \sum_{i=1}^{n} (m_i - \overline{m})^2}} \right)^2 \quad (2)$$

where $\boldsymbol{n}$ is the number of observations, $\boldsymbol{o_i}$ and $\boldsymbol{m_i}$ are the measured and simulated values, and $\overline{o}_i$ and $\overline{m}_i$ are the means of measured and calculated values, respectively.

(c) The root of Mean Square Error (RMSE), expressing the deviation between the simulated and the measured values. Such deviations are called residuals, and RMSE serves to concentrate them on a single predictive measure. The RMSE is given by the following equation:

$$RMSE = \sqrt{\frac{\sum_{i=1}^{n} (o_i - m_i)^2}{n}} \quad (3)$$

2.6. Model output post-processing

Reported model outputs refer to the salt wedge intrusion from April to November 2004. The salt-wedge intrusion length L_{30} (in km), defined as the upstream distance of the 30 psu isohaline from the seaward boundary and the salt wedge height $H_{15,0}$ (in m), defined as the vertical distance from seabed of the 15 psu isoline at the estuarine mouth, were determined (Seim et al., 2009).

3. Results

3.1. Model validation

The model produced fairly reliable results describing the hydrodynamics of the river and the salt wedge intrusion during summer 2004. Evaluation criteria illustrated relatively satisfactory model performance at five different points along the river, focusing at the salinity distribution in the water column. The salinity vertical profiles of the model were correlated with the profiles of in-situ salinity measurements, in five points along the river at the respective tidal phase of the sampling times (Table 3). Salinity r^2 reached 0.95, when all records are considered, with lower correlation at the river mouth. Upstream the river, correlation increases due to the formulation of the salt wedge. Maximum correlation is achieved at 3.1 km upstream the river mouth (r^2 =

0.97; RMSE = 3.98 psu; slope = 1.09). Slope values (>1) indicate slight model underestimation throughout the channel.

Indicative profiles of modeled/observed salinity (August 18, 2004; river discharge Q = 4 m^3/s; tidal range A = 0.30 m) are shown in Fig. 3. The height of the 15 psu isohaline, varies by ± 0.5 m between tidal phases and upstream locations. The distribution of salinity in the water column and along the river channel has been described with high accuracy by the hydrodynamic simulation. Minor declinations between simulation and in-situ measurements are observed; the higher discrepancy recorded at the surface layer (less than 5 psu). In the surface, the salinity estimated by the model is around 5 psu and in observations varies from 0 to 3 psu. In the bottom layers of the river mouth observation point, salinity gets the maximum value (up to 37 psu). During the flood tidal phase, the height of the salt wedge increases significantly (up to 30 cm), indicating the entry of sea water upstream the river. Moreover, during tidal ebb stratification becomes stronger and the height of the salt wedge decreases by approximately 30 cm. Further upstream, the effect of the tide appears negligible and stratification remains stable within the tidal cycle. Relatively high correlation is also shown comparing in-situ flow observations to hydrodynamic model results. Fig. 4 presents indicative water flow data and model results for the same tidal cycles in August 18, 2004. Positive values represent upstream directed velocities while negative designate the water flow from river to the sea. The model performed better in flood tidal phases, producing a surface freshwater layer (around 1 m thin) moving seawards with flow speed up to 0.18 m/s. Lower layers propagate to the opposite direction with maximum velocity of 0.17 m/s. The denser sea water enters the river from the lower layers pushing the salt wedge upstream the river, while fresh water flows to the opposite direction of the salt wedge. During ebb, the model produces seaward movement throughout the water column, having velocities up to 0.21 m/s at the surface layer. Overall, focusing on model result presented in Figs. 3 and 4, the upper layer of the river (about 1 m) with the lower salinity moves seaward and the lower layers move upstream, indicating the salt wedge intrusion. The model tends to underestimate (0.2 to 0.4 m/s) the water velocity values at the river surface in both flood and ebb tidal phases. Moreover, slight underestimation in bottom layer velocities (up to 0.2 m/s) is observed. The variation in river discharge between the E-Hype model and field observations (Haralambidou et al., 2010); $R^2 = 0.76$) could explain model flow underestimation, especially in the surface layers.

3.2. Strymon salt wedge formation

Model results analysis was performed on the simulations covering the summer 2004 (June to September). Salinity increases up to 37 psu at Strymon River mouth in early spring, attributed to the seasonal thinning of surface Black Sea Water, the entry and the vertical mixing with the more saline Levantine Intermediate Water at the shallow parts of Strymonikos Gulf. This gradual salinity rise in Strymonikos Gulf induces a higher horizontal density gradient, promoting salt intrusion along the river (Sylaios et al., 2006). Salt water enters the river channel in late May when river discharge is diminished. Intrusion occurs during the flood tidal phase on May 30, 2004, acting against the river discharge of 10 m^3/s. In June the salt wedge establishes along the river channel, intruding gradually further upstream during tidal springs. In less than 10 days, saline water of 30 psu appears approximately 3.6 km upstream the river due to the low river discharge (< 10 m^3/s).

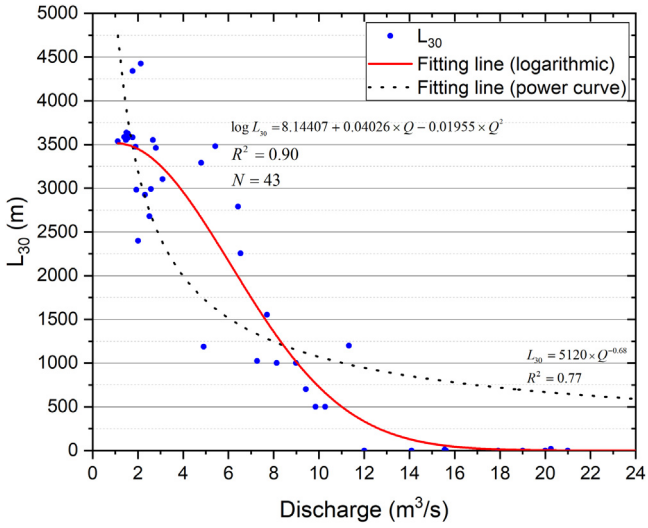

Fig. 6. Relation between salt-wedge length (L_{30}) and river discharge (Q).

3.3. Strymon salt wedge length

L_{30}-index describes the length of the wedge in relation to the longitudinal mixing processes along the sharp wedge interface. The length of the salt wedge is strongly related to the river discharge and tidal dynamics. Fig. 5 presents the temporal change in L_{30} in relation to the tidal and river flow conditions. During the summer 2004 simulation the mean L_{30}-value reaches 3.6 km upstream. However, a sharp rise in L_{30} was observed from July 30, 2004 to August 12, 2004 up to the maximum intrusion length of 4.6 km upstream. The salt wedge, driven by the tidal springs prevailing on August 5, 2004, reached the highest L_{30} intrusion length under low river flow conditions of about 3 m^3/s.

Minimum intrusion lengths (L_{30}) in the summer were simulated on June 19, 2004, July 01, 2004 and August 18, 2004, coinciding with a slight increase in freshwater discharge (> 3 m^3/s) and tidal neaps (A ~ 0.14 m). In these dates, L_{30} was limited to 2.2 km upstream the river mouth (Fig. 5). In early September 2004 the saline intrusion length (L_{30}) gradually declines as the salt wedge is gradually flushed out of the river mouth. However, part of the salt wedge was separated from its main core and was entrapped at the deeper parts of the riverbed. Such entrapment and presence of residual salt-wedge water was also observed by Haralambidou et al. (2010), approximately 4 km upstream, attributed to complex bottom topography. Model results showed that this water mass became eventually completely mixed during the late days of October 2004.

The relationship between L_{30} produced by the validated model and the variability in Strymon River discharge is best-approached by a logarithmic function (Fig. 6):

$$\log L_{30} = 8.14407 + 0.04026 \times Q - 0.01955 \times Q^2 \quad (4)$$

This function describes better the L_{30} variability ($R^2 = 0.90$) along the lower Strymon channel and removes the wedge under increased river discharge conditions (>16 m^3/s).

Testing the power curve law, reported by many previous investigators, a simpler function was derived, as:

$$L_{30} = 5120 \times Q - 0.68 \quad (5)$$

The produced power curve is less successful in L_{30}-representation ($R^2 = 0.77$). The power index (−0.68) appears significantly lower than those reported by Krvavica and Ružić

Table 3
Statistical parameters for salinity validation along the Strymon River.

	At the river mouth	1 km upstream	2 km upstream	3.1 km upstream	4.1 km upstream
Number of observations	178	194	197	249	42
Slope (γ)	1.07	1.13	1.12	1.09	1.13
R-Square	0.93	0.96	0.94	0.97	0.96
RMSE (psu)	5.88	4.42	5.30	3.98	4.23

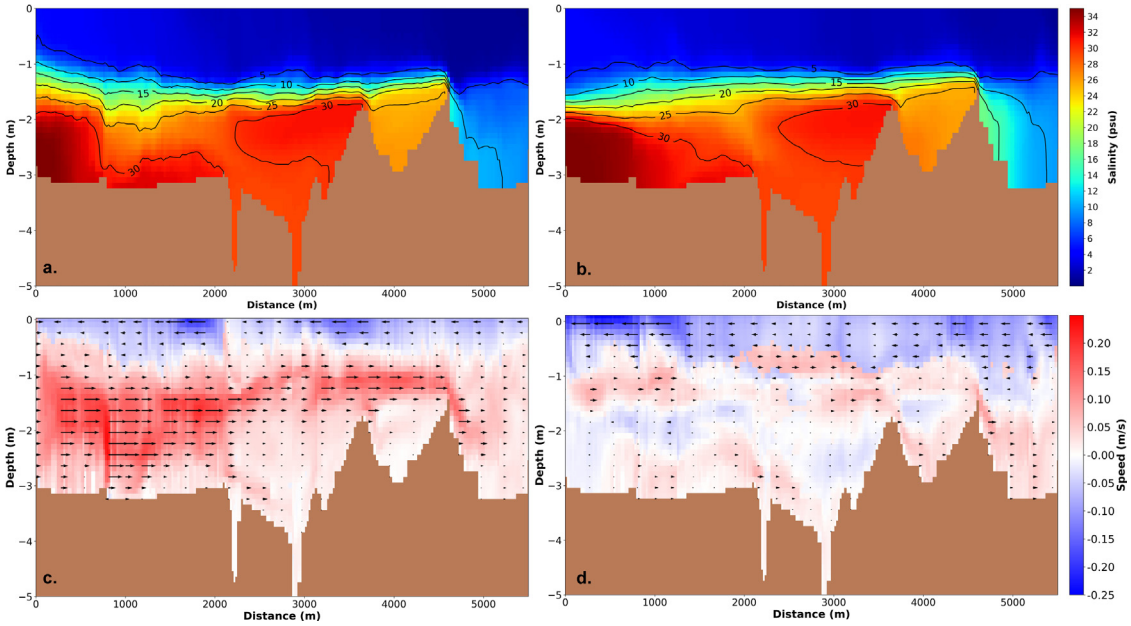

Fig. 7. Longitudinal distribution of (a, b) water salinity, and (c, d) water flow speed during the spring tide on July 16, 2004 (Q = 2 m^3/s; A = 0.28 m). Graphs on the left represent the flood tide and on the right the ebb tidal phase. The river boundary is located to the right of figure.

(2020) (exponent −2.03) and Geyer and Ralston (2011) (exponents from −2.5 to −2.0), since these were derived for higher river flows (>250 m^3/s), signifying the importance of river discharge in highly-stratified flows. Ralston et al. (2010) reported an exponent of −0.19 for the mesotidal Merrimack River. Poggioli and Horner-Devine (2015) noted that such simple power-law models describe the physics of salt wedges in the absence of tidal and topographic variation.

Further, when the salt intrusion length L_{30} depends not only on river discharge (Q), but also on the tidal variability (SWL), a more complex function was fitted:

$$L_{30} = 4647.04 \times Q^{-0.53} + 43.14 \times SWL \quad (6)$$

having $R^2 = 0.83$ (n = 43). This function is directly comparable to that reported by Krvavica et al. (2016) for the microtidal Rječina River Estuary in Croatia.

3.4. Salt wedge intra-tidal and fortnight dynamics

Salt wedge intrusion in Strymon River was studied in two tidal periods (spring and neap) and their two tidal phases (flood and ebb) under low river discharge (Q ∼ 2 m^3/s). Fig. 7 shows the distribution of salinity and the total speed modeled in tidal spring along the longitudinal Strymon River transect (July 16, 2004; Q = 2 m^3/s; A = 0.28 m). During the flood phase (Fig. 7a), sea water (∼37 psu) enters the river mouth, pushing the wedge upstream, inducing increased vertical shear. The main body of the wedge flows upstream reaching values up to 0.25 m/s, while the surface layer moves from the river to the sea (speed up to 0.20 m/s). During ebb, the surface flow approximates 0.2 m/s at the mouth, moving seaward. Significant speed values are also observed at the upper layers of the salt wedge, indicating a slight retreat of salt water from the salt wedge to the sea. The speed diminishes to near zero values at the bottom layer, retaining the upstream flow direction (Fig. 7b).

In neap tide (July 10, 2004; Q ∼ 2 m/s; A = 0.10 m), limited sea water volume enters the river channel, resulting in the reduction of salt wedge height ($H_{15,0}$ =∼1.3 m). Mixing is inhibited along the river mouth and the wedge seems better formulated with a sharp interface. In flood phase (Fig. 8a), higher flow speeds directed from sea to the river are observed at the interface; at the river mouth (up to 0.085 m/s) and at 3.2 km upstream (up to 0.1 m/s). During ebb almost zero velocity values are reported at the interface and flow reversal prevails at the area near the open boundary (Fig. 8b).

4. Discussion

Strymon River mouth is a micro-tidal system characterized by the presence of a salt-wedge propagating upstream during the summer months when low freshwater flow prevails. Similar salt-wedge patterns have been reported along other Mediterranean rivers. Indicatively, in Ebro river (Spain) the length of the salt wedge is observed up to 32 km upstream (Ibañez et al. 1997; (Sierra et al., 2002), in Neretva river salt water is observed over 23 km upstream the river mouth (Ljubenkov and Vranješ, 2012), in Jadro salt water intrusion appears over 1 km (Ljubenkov, 2015) and in Rječina intrudes just under 1 km (Krvavica et al., 2017b).

A three-dimensional hydrodynamic model (ELCOM) was configured to describe the hydrodynamic characteristics of the last 8 km of Strymon River flow. The model was calibrated and validated based on previous field surveys (June to August 2003

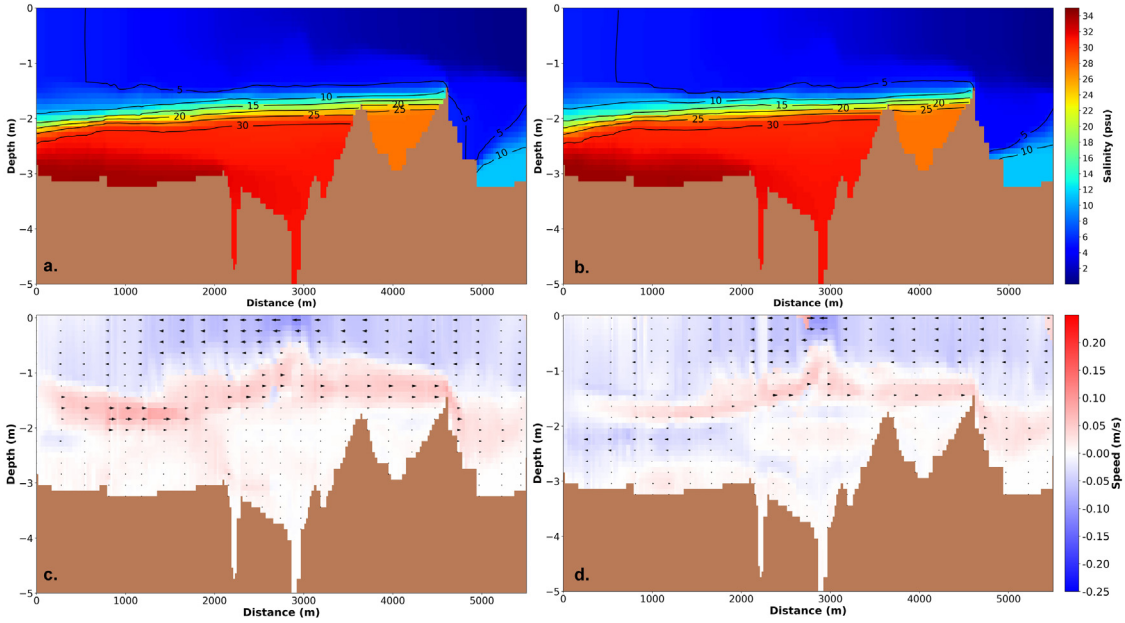

Fig. 8. Longitudinal distribution of (a, b) water salinity, and (c, d) water flow speed during the neap tide on July 10, 2004 (Q = 2 m^3/s; A = 0.10 m). Graphs on the left represent the flood tide and on the right the ebb tidal phase. The river boundary is located to the right of figure.

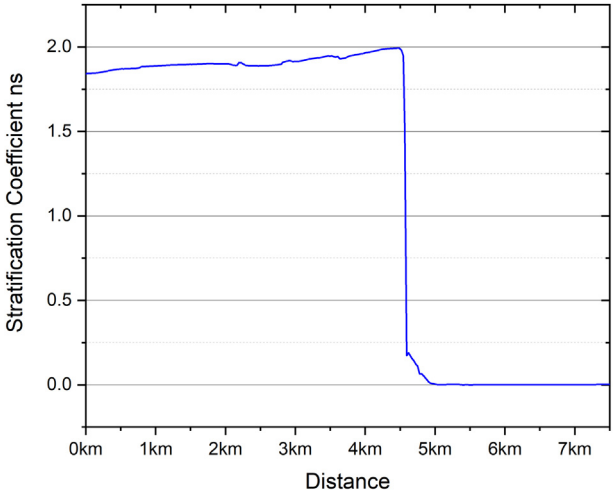

Fig. 9. Mean variability of the stratification indicator n_S along Strymon River lower channel on August 9, 2019.

and 2004) (Haralambidou et al., 2010). Model findings suggest that salt wedge dynamics along the river channel are principally driven by Strymon River discharge. The salt wedge is observed from June to September, intruding up to 4.6 km when the river discharge in the river mouth area is low (Q < 12 m^3/s). As shown by the models (Eqs. (4)–(6)) introduced to describe the salt wedge intrusion length (L_{30}), river discharge plays a major role governing its dynamics, although during the summer period, when Strymon River flow is constantly low, the impact of tidal action in the length of wedge intrusion is observed. Similarly, in the Neretva river the salt wedge penetrates upstream up to 23 km in low river flow during summer months and flushes out when the river discharge exceeds 500 m^3/s (Ljubenkov and Vranješ, 2012).

Additionally, the intra-tidal dynamics in combination with the low river flow affect the geometry (length and thickness) of the salt wedge and the river column stratification. The most significant change in salt wedge interface is observed under spring tide and low river discharge rates, when the sea level oscillates with an amplitude of 0.30 m. The salt-wedge length (L_{30}) fluctuated up to 4.6 km and the salt-wedge height at the mouth ($H_{15,0}$) up to 0.9 m between the maximum flood and the maximum ebb tidal phase. Neap cycles illustrated negligible intra-tidal changes in the salt wedge geometry.

Another factor that affects the salt wedge shape is the river-bed morphology, where mixing processes are primarily driven by bottom shear, with interfacial stress playing a secondary role (Nepf and Geyer, 1996; Zhou, 1998; Trowbridge et al., 1999). In Strymon River, two shallow submerged sills are formed at 3.6 km and 4.6 km upstream of the river mouth, inhibiting salt wedge propagation and limiting its intrusion up to the 4.6 km-limit. Submerged sills blocking the salt wedge propagation were also found in the Rječina River Estuary (Krvavica et al., 2017b).

To understand the water column characteristics of the lower Strymon River channel, the n_S indicator was produced based on the results of the numerical model, expressed as (Tuin, 1991):

$$n_s = \frac{\delta S}{S'_m} \tag{7}$$

where $\delta S = S_{bott} - S_{surf}$, $S'_m = 0.5 \times (S_{bott} + S_{surf})$, with S_{surf} and S_{bott} the salinity at the surface and bottom of the water column, respectively. The stratification indicator n_S takes near zero values at the riverine part of the channel due to the presence of well-mixed water column. Along the remaining channel, from the seaward boundary until the salt wedge limit of 4.6 km upstream, n_S was consistently found above 1.0, ranging between 1.5 at the river mouth to 2.0 at the upper saline intrusion limit, indicating the presence of a stationary, well-stratified salt wedge (Fig. 9). In accordance to MacCready and Geyer (2001) in the Fraser river, flood is the most productive period for vertical salt flux leading to the elongation of the isohalines. Additionally, results from both hydrodynamic model and Haralambidou et al. (2010) study illustrate that the minimum value in the stratification index n_S occurred at the commencement of the flood tidal phase, while higher stratification is observed at the end of flood to the commencement of ebb period.

Additionally, the strong vertical stratification in the river was also indicated by estimating the buoyancy frequency (N^2), by

Brunt-Vaisala:

$$N^2 = -\frac{g}{\rho_0}\frac{\partial \rho}{\partial z} \tag{8}$$

where ρ_0 is the reference density of sea water. In Strymon, the surface-to-bottom density varies from 1,000 to 1,026 kg m^{-3}, thus the squared buoyancy frequency ranged typically from 0.04 to 0.08 s^{-2}, with a typical depth-averaged N^2-value of 0.07 s^{-2}. However, close to the wedge interface, the local N^2-value reaches 0.25 s^{-2}. According to Geyer et al. (2008), salt wedge estuaries may have values up to 0.3 s^{-2}. Similar squared buoyancy frequency values are observed in Hudson river estuary (Peters, 1997).

To explore further the bidirectional flow dynamics, the non-dimensional freshwater Froude number (F_f) was introduced, as:

$$F_f \equiv \frac{Q}{b_0\sqrt{g_0' h_0^3}} \tag{9}$$

expressing the barotropic flow induced in the river channel due to sea-surface elevation at the riverine boundary. Q is river discharge, b_0 is the channel width at the ocean boundary, g_0' is the reduced gravitational acceleration, considering buoyancy ($g_0' = g\Delta\rho/\rho_0$), with $\Delta\rho$ being the difference between layer densities, and h_0 is the water depth at the ocean boundary. Considering Strymon River mouth as a sloped, prismatic channel, having horizontal bed slope $\alpha = 0.062$ and along-channel convergence ratio $R_C = b_0/b_R = 2.25$ (b_R is the channel width at the upstream river boundary), the non-dimensional salt wedge intrusion length L_* is defined, as:

$$L_* = \frac{C_D L_{30}}{h_0} \tag{10}$$

where C_D is the drag bottom coefficient, defined in calibration as $C_D = 0.002$. Through the theoretical analysis of Poggioli and Horner-Devine (2015), the relative influence of seabed frictional effects to topographic and bathymetric along-channel changes on the salt wedge intrusion length L_* is addressed by the C_D/α (C_D/α for Strymon is 0.032) and R_C-ratios. Fig. 10 illustrates the variability of the non-dimensional salt wedge intrusion length over the densimetric Froude number, on a daily basis for year 2004 (June to September), based on the ELCOM model results. The L_* vs F_f-curve proves the previously reported theoretical considerations that channel convergence has a significant effect on Strymon salt wedge intrusion length. Based on this analysis, a function linking the non-dimensional intrusion length and the freshwater Froude number was fitted on model results, as:

$$L_* = 2.65 \times (1 + F_f)^{-10.41} \tag{11}$$

having high reliability ($R^2 = 0.90$).

Water renewal along the river channel depends highly on the river discharge and the tidal force acting along the river mouth. Furthermore, it is also affected by seabed morphology. More specifically, the existence of two submerged sills and the presence of two deeper channel parts influence significantly the water retention time. Retention time (RT) is an important parameter for the environmental management of the study area. According to Dyer (1997), retention time is defined as the time taken to replace the existing freshwater in the estuary at a rate equal to river discharge. The model calculates the time each water parcel spends within the computational grid. RT provides an understanding of the dynamics of chemical substances dissolved in the water, especially at the bottom stagnant layer, assessing the negative consequences for the water quality. In the Strymon River mouth RT varies from 1 to 20 days. Under low river discharge, the fresh water flows on the surface layer towards the open sea

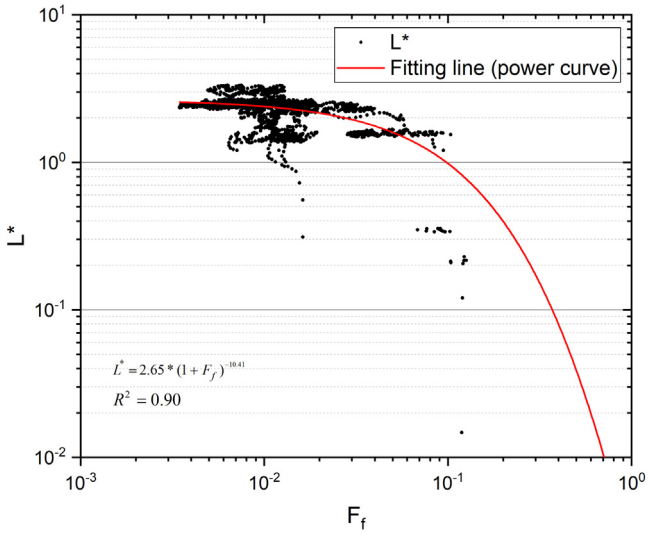

Fig. 10. Model linking the non-dimensional intrusion length L_* to the freshwater Froude number F_f, based on the results of the hydrodynamic simulation.

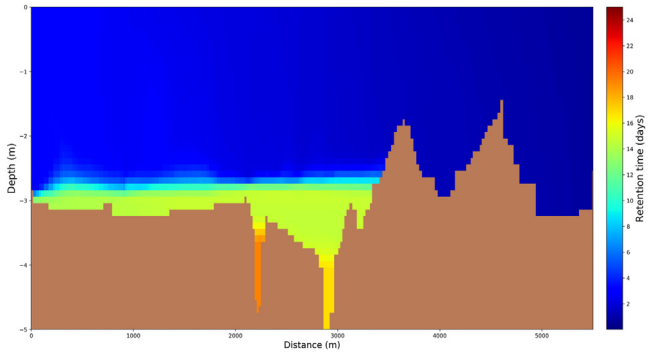

Fig. 11. Distribution of retention time along the Strymon River lower channel as computed by ELCOM on September 25, 2004 (Q = 9 m^3/s; A = 0.15 m).

exerting limited force to the salt wedge. The retention time of the salt wedge water varies from 10 to 20 days with the maximum value observed at the deeper parts of the river mouth (Fig. 11). The slow water renewal in these areas is directly related to the low concentration of dissolved oxygen in the water column and the riverbed, highlighted on August 22, 2004 by in-situ observations (Haralambidou et al., 2010). The dissolved oxygen content recorded at the deeper Strymon River parts was lower than 4 mg/l, affected by the slow water renewal. This low dissolved oxygen value favors the remineralization of phosphorus and trace metals from riverbed to the water column (Haralambidou et al., 2010).

5. Conclusions

The simulation of salt water intrusion, the salt wedge formation and establishment along the channel were studied applying a three-dimensional model along the Strymon River mouth. The model was calibrated and validated based on sampling campaigns over the spring/summer months of 2003 and 2004. Model results allowed the study of salinity and velocity profiles, the strength of stratification along-channel and the salt wedge morphology during different hydrographic conditions. Overall, a stationary, well-stratified salt wedge is observed in summer months, when river discharge diminishes as freshwater is used upstream for agriculture.

The three-dimensional model applied herein produced fairly accurate results and captured satisfactorily the shape of the arrested salt-wedge in the irregular geometry of Strymon River mouth. Hydrodynamic model results explained adequately environmental issues reacted to salt wedge intrusion, such as bottom anoxia and nutrients and metals remineralization along the river. The spring/summer low river discharge, acting in parallel to the tidal action favored the salt wedge intrusion up to 4.6 km upstream. The morphology of the river topography and bathymetry is also a key factor controlling the shape and the length of the salt wedge, while entrapping water at deeper points. Landward width constriction allows the saline intrusion to penetrate further up-estuary than it would have otherwise. Model results were used to test theoretical considerations developed for sloped and convergent channels by previous researchers.

These results highlight the need for further studies, especially in the field of operational numerical modeling and forecasting to produce real-time reliable salinity and water flow profiles. Such operational system will have the capacity to respond in any change of external conditions affecting the system, thus leading to proper river management decisions.

CRediT authorship contribution statement

Konstantinos Zachopoulos: Data curation, Formal analysis, Investigation, Methodology, Project administration, Visualization, Writing - original draft. **Nikolaos Kokkos:** Data curation, Formal analysis, Investigation, Methodology, Software, Visualization, Writing - original draft. **Georgios Sylaios:** Conceptualization, Methodology, Resources, Supervision, Validation, Writing - review & editing.

Declaration of competing interest

The authors declare that they have no known competing financial interests or personal relationships that could have appeared to influence the work reported in this paper.

Acknowledgments

The research leading to these results received funding from the European Union Horizon 2020 Program (H2020-BG-12-2016-2) under grant agreement 727277 - ODYSSEA (Towards an integrated Mediterranean Sea Observing System).

References

Barlow, P., 2003. Saltwater intrusion from the Delaware River during drought-implications for the effect of sea-level rise on coastal aquifers. Ground water in freshwater–saltwater environments of the Atlantic coast. US Geol. Surv., Reston 4, 6–48.

Casulli, V., Cheng, R.T., 1992. Semi-implicit finite difference methods for three-dimensional shallow water flow 15, 629-648. http://dx.doi.org/10.1002/fld.1650150602.

Chanson, H., 2004. Environmental Hydraulics for Open Channel Flows. Elsevier Butterworth-Heinemann, Burlington.

Chen, X., Flannery, M.S., Moore, D.L., 2000. Response times of salinity in relation to changes in freshwater inflows in the lower hillsborough river, Florida. Estuaries 23, 735–742. http://dx.doi.org/10.2307/1352899.

D'Adamo, N., Lukatelich, R.J., 1985. Water Quality of the Murray River Estuary. Centre for Water Research, University of Western Australia, Nedlands, W.A.

Dassenakis, M., Scoullos, M., Gaitis, A., 1997. Trace metals transport and behaviour in the mediterranean estuary of Acheloos river. Mar. Pollut. Bull. 34, 103–111. http://dx.doi.org/10.1016/s0025-326x(96)00062-8.

Donnelly, C., Andersson, J.C.M., Arheimer, B., 2016. Using flow signatures and catchment similarities to evaluate the E-HYPE multi-basin model across Europe. Hydrol. Sci. J. 61, 255–273. http://dx.doi.org/10.1080/02626667.2015.1027710.

Dyer, K.R., 1997. Estuaries: A Physical Introduction, second ed. Wiley.

Fischer, H.B., List, J.E., Koh, C.R., Imberger, J., Brooks, N.H., 1979. Mixing in Inland and Coastal Waters. Academic Press.

Geyer, W.R., MacCready, P., 2014. The estuarine circulation. Annu. Rev. Fluid Mech. 46, 175–197. http://dx.doi.org/10.1146/annurev-fluid-010313-141302.

Geyer, W.R., Ralston, D., 2011. The dynamics of strongly stratified estuaries. In: Treatise on Estuarine and Coastal Science, first ed. Academic Press, Amsterdam, pp. 37–51.

Geyer, W.R., Scully, M.E., Ralston, D.K., 2008. Quantifying vertical mixing in estuaries. Environ. Fluid Mech. 8 (5), 495–509. http://dx.doi.org/10.1007/s10652-008-9107-2.

Graas, S., Savenije, H.H.G., 2008. Salt intrusion in the Pungue estuary, Mozambique: effect of sand banks as a natural temporary salt intrusion barrier. Hydrol. Earth Syst. Sci. Discuss. 5, 2523–2542. http://dx.doi.org/10.5194/hessd-5-2523-2008.

Hansen, D.V., Rattray Jr, M., 1966. Gravitational circulation in straits and estuaries. J. Mar. Res. 23, 104–122.

Haralambidou, K.I., Sylaios, G.K., Tsihrintzis, V.A., 2003. Testing alternatives for salt wedge management in an estuary with the use of monitoring and mathematical model. Global Nest: Int. J. 2, 107–118. http://dx.doi.org/10.30955/gnj.000295.

Haralambidou, K., Sylaios, G., Tsihrintzis, V.A., 2010. Salt-wedge propagation in a Mediterranean micro-tidal river mouth. Estuar. Coast. Shelf Sci. 90, 174–184. http://dx.doi.org/10.1016/j.ecss.2010.08.010.

Haralambidou, K.I., Tsihrintzis, V.A., Sylaios, G.K., Akratos, C., 2005. Seasonal and spatial characteristics of water quality in the estuary of Strymon River. J. Mar. Environ. Eng. 7, 231–239.

Hodges, B.R., 2000. Numerical Techniques in CWR-ELCOM (code release v. 1). CWR Manuscript WP, p. 1422.

Hodges, B., Dallimore, C., 2006. Estuary, Lake and Coastal Ocean Model: ELCOM V2. 2 Science Manual. Centre for Water Research, University of Western Australia.

Hume, T.M., Snelder, T., Weatherhead, M., Liefting, R., 2007. A controlling factor approach to estuary classification. Ocean Coast. Manag. 50, 905–929. http://dx.doi.org/10.1016/j.ocecoaman.2007.05.009.

Ibañez, C., Pont, D., Prat, N., 1997. Characterization of the Ebre and Rhone estuaries: A basis for defining and classifying salt-wedge estuaries 42, 89–101. http://dx.doi.org/10.4319/lo.1997.42.1.0089.

Kasai, A., Kurikawa, Y., Ueno, M., Robert, D., Yamashita, Y., 2010. Salt-wedge intrusion of seawater and its implication for phytoplankton dynamics in the Yura Estuary, Japan. Estuar. Coast. Shelf Sci. 86, 408–414. http://dx.doi.org/10.1016/j.ecss.2009.06.001.

Krvavica, N., Kožar, I., Travaš, V., Ožanić, N., 2017a. Numerical modelling of two-layer shallow water flow in microtidal salt-wedge estuaries: Finite volume solver and field validation. J. Hydrol. Hydromech. 65 (1), 49–59. http://dx.doi.org/10.1515/johh-2016-0039.

Krvavica, N., Ružić, I., 2020. Assessment of sea-level rise impacts on salt-wedge intrusion in idealized and Neretva River Estuary. Estuar. Coast. Shelf Sci. 234, 106638. http://dx.doi.org/10.1016/j.ecss.2020.106638.

Krvavica, N., Travaš, V., Ožanić, N., 2016. A field study of interfacial friction and entrainment in a microtidal salt-wedge estuary. Environ. Fluid Mech. 16 (6), 1223–1246. http://dx.doi.org/10.2112/JCOASTRES-D-16-00053.1.

Krvavica, N., Travaš, V., Ožanić, N., 2017b. Salt-wedge response to variable river flow and sea-level rise in the Microtidal Rječina River Estuary, Croatia. J. Coast. Res. 33, 802–814. http://dx.doi.org/10.2112/jcoastres-d-16-00053.1.

Lindström, G., Pers, C., Rosberg, J., Strömqvist, J., Arheimer, B., 2010. Development and testing of the HYPE (Hydrological Predictions for the Environment) water quality model for different spatial scales. Hydrol. Res. 41, 295–319. http://dx.doi.org/10.2166/nh.2010.007.

Ljubenkov, I., 2015. Hydrodynamic modeling of stratified estuary: case study of the Jadro River (Croatia), 63, 29–37, http://dx.doi.org/10.1515/johh-2015-0001.

Ljubenkov, I., Vranješ, M., 2012. Numerical model of stratified flow - Case study of the Neretva riverbed salination (2004). Građevinar 64 (2), 101–112. http://dx.doi.org/10.14256/JCE.639.2011.

MacCready, P., Geyer, W.R., 2001. Estuarine salt flux through an isohaline surface. J. Geophys. Res.: Oceans 106, 11629–11637. http://dx.doi.org/10.1029/2001jc900006.

Marti, C., Imberger, J., 2015. A real-time management system for the Swan-Canning River Basin and its receiving waters, Western Australia, Australia, E-proceedings of the 36th IAHR World Congress.

McAnally, W.H., Pritchard, D.W., 1997. Salinity control in Mississippi river under drought flows 123, 34–40. http://dx.doi.org/10.1061/(ASCE)0733-950X(1997)123:1(34).

McAuliffe, T., Lukatelich, R., Hill, N., 1993. The role of sediments in phosphorus cycling in the Swan River Estuary, Swan River Trust—The Future, Workshop Proceedings, pp. 75–87.

Monbet, Y., 1992. Control of phytoplankton biomass in estuaries: A comparative analysis of microtidal and macrotidal estuaries 15, 563–571. http://dx.doi.org/10.2307/1352398.

Nepf, H.M., Geyer, W.R., 1996. Intratidal variations in stratification and mixing in the Hudson estuary 101, 12079–12086. http://dx.doi.org/10.1029/96jc00630.

Parissis, A., Sylaios, G., Tsihrintzis, V., 2001. A numerical model for the study of salt intrusion at Strymon River mouth, Northern Greece. In: Proceedings of the First International Congress on Ecological Protection of Planet Earth, pp. 5–8.

Peters, H., 1997. Observations of stratified turbulent mixing in an estuary: Neap-to-spring variations during high river flow. Estuar. Coast. Shelf Sci. 45 (1), 69–88. http://dx.doi.org/10.1006/ecss.1996.0180.

Poggioli, A.R., Horner-Devine, A.R., 2015. The sensitivity of salt wedge estuaries to channel geometry. J. Phys. Oceanogr. 45 (12), 3169–3183. http://dx.doi.org/10.1175/JPO-D-14-0218.1.

Pritchard, D.W., 1967. Observations of circulation in coastal plain estuaries. In: Lauff, G.H. (Ed.), Estuaries. American Association for the Advancement of Science Publication, Washington DC, pp. 37–44.

Ralston, D.K., Geyer, W.R., Lerczak, J.A., Scully, M., 2010. Turbulent mixing in a strongly forced salt wedge estuary. J. Geophys. Res.: Oceans 115 (C12), C12024. http://dx.doi.org/10.1029/2009JC006061.

Ranmadugala, S.B.H., 2004. Influence of Seasonal Sea Level Variability on Salt-Water Intrusion in Kelani River Basin.

Robson, B.J., Hamilton, D.P., 2004. Three-dimensional modelling of a Microcystis bloom event in the Swan River estuary, Western Australia. Ecol. Model. 174, 203–222. http://dx.doi.org/10.1016/j.ecolmodel.2004.01.006.

Sargent, F.E., Jirka, G.H., 1987. Experiments on saline wedge 113, 1307–1323. http://dx.doi.org/10.1061/(ASCE)0733-9429(1987)113:10(1307).

Scoullos, M.J., Oldfield, F., 1986. Trace metal and magnetic studies of sediments in greek estuaries and enclosed gulfs. Mar. Chem. 18, 249–268. http://dx.doi.org/10.1016/0304-4203(86)90012-5.

Seim, H.E., Blanton, J.O., Elston, S.A., 2009. The effect of secondary circulation on the salt distribution in a sinuous coastal plain estuary: Satilla River, GA, USA. Cont. Shelf Res. 29, 15–28. http://dx.doi.org/10.1016/j.csr.2008.03.018.

Sierra, J.P., Sánchez-Arcilla, A., Figueras, P.A., Gonzalez Del Rio, J., Rassmussen, E.K., Mösso, C., 2004. Effects of discharge reductions on salt wedge dynamics of the Ebro River. River Res. Appl. 20, 61–77.

Sierra, J.P., Sánchez-Arcilla, A., González Del Río, J., Flos, J., Movellán, E., Mösso, C., Martínez, R., Rodilla, M., Falco, S., Romero, I., 2002. Spatial distribution of nutrients in the Ebro estuary and plume. Cont. Shelf Res. 22, 361–378. http://dx.doi.org/10.1016/S0278-4343(01)00061-9.

Sylaios, G., Koutrakis, E., Kallianiotis, A., 2006. Hydrographic variability, nutrient distribution and water mass dynamics in Strymonikos Gulf (Northern Greece). Cont. Shelf Res. 26, 217–235. http://dx.doi.org/10.1016/j.csr.2005.11.002.

Trowbridge, J.H., Geyer, W.R., Bowen, M.M., Williams, A.J., 1999. Near-bottom turbulence measurements in a partially mixed estuary: Turbulent energy balance, velocity structure, and along-channel momentum balance. J. Phys. Oceanogr. 29, 3056–3072. http://dx.doi.org/10.1175/1520-0485(1999)029<3056:Nbtmia>2.0.Co;23056:Nbtmia>2.0.Co;2.

Tuin, H., 1991. Guidelines on the Study of Seawater Intrusion Into Rivers. Unesco.

Valle-Levinson, A., 2010. Contemporary Issues in Estuarine Physics. Cambridge University Press, Cambridge.

Vieira, M.E.C., Bordalo, A.A., 2000. The Douro estuary (Portugal): a mesotidal salt wedge. Oceanol. Acta 23, 585–594. http://dx.doi.org/10.1016/s0399-1784(00)01107-5.

Watanabe, K., Kasai, A., Antonio, E.S., Suzuki, K., Ueno, M., Yamashita, Y., 2014. Influence of salt-wedge intrusion on ecological processes at lower trophic levels in the Yura Estuary, Japan. Estuar. Coast. Shelf Sci. 139, 67–77. http://dx.doi.org/10.1016/j.ecss.2013.12.018.

Zhou, M., 1998. Influence of bottom stress on the two-layer flow induced by gravity currents in estuaries. Estuar. Coast. Shelf Sci. 46, 811–825. http://dx.doi.org/10.1006/ecss.1998.0306.